Talanta 118 (2014) 304–311

Contents lists available at ScienceDirect

Talanta

journal homepage: www.elsevier.com/locate/talanta

Theoretical and experimental study of sensing triacetone triperoxide (TATP) explosive through nanostructured TiO_2 substrate

Rupashree S. Ray [a], Biplab Sarma [a], Swomitra Mohanty [a,b], Mano Misra [a,b,*]

[a] Metallurgical Engineering, University of Utah, Salt Lake City, UT 84112, USA
[b] Chemical Engineering, University of Utah, Salt Lake City, UT 84112, USA

ARTICLE INFO

Article history:
Received 30 June 2013
Received in revised form
28 September 2013
Accepted 30 September 2013
Available online 22 October 2013

Keywords:
TATP
Explosive
Computational Modeling
Sensor
TiO_2 nanotube

ABSTRACT

The present study focuses on understanding of the principle of interaction of explosive molecule triacetonetriperoxide (TATP) with metal sensitized TiO_2 nanotube composite material through theoretical modeling. This effort has also been extended in developing a laboratory scale sensor set up to detect TATP based on comprehensive computational modeling outcome and subsequent experimentation. Sensing mechanism depends on the nature of metal, where the TATP interaction with metal functionalized TiO_2 prompts a change in conductivity of the sensor platform. Therefore, a metal with higher affinity towards TATP would enhance the conductance, thereby promoting the efficiency of the sensor platform. DFT methodology has been used to identify metal with high affinity to TATP. It was found that Co^{2+} metal ion shows significantly higher affinity towards TATP, selected from an array of metal ions with different valency, from monovalent to tetravalent. The preliminary experimental data also suggests that Co^{2+} ion detects TATP by inducing a change in conductivity of the sensor substrate.

1. Introduction

In recent years, peroxide based explosives such as triacetone triperoxide (TATP) is the most potent and dangerous and it is the ammunition of choice for terrorism in different parts of the world. TATP has very high vapor pressure and it is very susceptible to heat, friction, and shock leading to explosion. Peroxide based explosive, TATP pose a significant risk owing to its ease of fabrication and difficulty in direct detection.

Various researchers have reported different methodologies to detect TATP [1–3]. Sensor devices for explosive detection that are used currently are not applicable for peroxide based explosives, owing to their thermolability and absence of chromophoric groups. Techniques that are able to detect peroxide based explosives generally require bulky and expensive instrumentation, need extensive sample preparation, need direct contact, and cannot detect TATP in the gas phase. Till date the conventional detectors fail to detect the new peroxide based explosives. There have been considerable experimental efforts to develop a sensor for these explosive materials [1–6]. Yet, so far there has not been any significant success in advancement of a sensor device for practical application. Several studies suggest that the interference of metal ions coated on metal oxide arrays is capable for TATP detection [7–9]. An important limitation of TATP sensor development appears to be the lack of theoretical understanding of the underlying mechanisms. Here we are proposing to conduct a comprehensive theoretical study and then develop a sensor based on functionalized metal oxide nanotubular arrays. It is expected that the sensor will meet all the above stated criteria and also can be inexpensive.

The advent of solid state sensors based on the metal oxide arrays or coated quartz sensors put forth a new opportunity for detection of peroxide based explosives. The devices are based on the requirement of developing a coating or a layer that will selectively and specifically bind the peroxide molecules that subsequently give a positive response by changing the physical and chemical behavior of the metal oxide array [10].

This paper outlines the fundamental understanding of underlying mechanism of the interaction of TATP with metal sensitized titanium dioxide nanotubular arrays (TiO_2–NT) and that eventually leads to fabrication of peroxide based explosive materials detection system. The system for our sensing platform is based on metal sensitized TiO_2-NT arrays, where the nature of metal determines the TATP detection. The metal–TATP interaction prompts a change in the electrical resistivity of the device, which basically underlines the process for sensing mechanism. Therefore, understanding the microscopic interaction underlying the detection mechanism of explosive molecule TATP is very crucial in developing an efficient sensor device.

In this particular field, one dimensional metal oxide nano materials have shown promising potential owing to their semiconducting

* Corresponding author at: Metallurgical Engineering, University of Utah, Salt Lake City, UT 84112, USA. Tel.: +1 801 581 6386; fax: +1 801 581 4937.
E-mail address: Mano.Misra@utah.edu (M. Misra).

0039-9140/$ - see front matter © 2013 Elsevier B.V. All rights reserved.
http://dx.doi.org/10.1016/j.talanta.2013.09.057

nature, corrosion resistant property, ease of preparation and handling by anodization method [11-21]. Nanotubular architecture being highly ordered enhanced field-effect carrier mobility, together with increased electrical conductivity and reduced activation energy for electrical conduction. This study shows the feasibility to develop a solid state sensor for detection of TATP based on metal functionalized TiO_2–NT arrays with specific emphasis on the fundamental analysis of the actual mechanism of such a sensor. The metal–TATP interaction prompts a change in the electrical resistivity of the sensor platform. Hence, selection of suitable metal ion to be functionalized with TiO_2–NT is very important. Using Zn^{2+} as a candidate metal ion functionalized on TiO_2–NT, previously detection of TATP has been performed experimentally [14]. However, the selection of metal ions has to be done systematically and a large array of experiments considering different oxidation state of the metal needs to be performed. This process is time consuming as well as expensive. Moreover, explosive material TATP need to be handled with utmost care. Hence, these serious issues can be considered only through a comprehensive theoretical understanding of binding mechanisms of various metal ions to TATP.

2. Computational studies

The sensor device is based on metal sensitized TiO_2–NT, where the nature of metal determines the TATP detection. Hence, our preliminary computational approach was largely applied towards the study of metal interaction with TATP and identification of the suitable metals with strong affinity to TATP. The evaluation and identification was performed for a set of metal ions of different valency such as: monovalent: Li^{1+}, Cu^{1+}, divalent: Fe^{2+}, Ni^{2+}, Cr^{2+}, Co^{2+}, Pb^{2+}, Zn^{2+}, trivalent: In^{3+}, Co^{3+}, Cr^{3+}, Sb^{3+}, and tetravalent: Pd^{4+} and Pt^{4+} selected on the basis of Hard–Soft–Acid–Base principle. The computational study of above metal cations with TATP is conducted using density functional theory (DFT) as implemented in Gaussin09 program package [22]. The calculations are carried out with hybrid exchange-correlation functional B3LYP which is found to perform well in predicting the chemical applications such as structure and energetics. Transition metals were decribed by small core ECP SDD i.e. the Stuttgart-Dresden ECP as demonstrated in the recent computational study by Xu et al. [23] that relativistic small-core ECPs with the corresponding valence basis sets are quite appropriate in describing the transition metal ion properties. The ligand (TATP) atoms i.e. C, O, H were described by the 6–31 G+(2d) basis set. Geometry optimizations were performed for different metal–TATP complexes without any symmetry restrictions and for each structure, we carried out a normal mode analysis in the gas phase to confirm their character as local minimum. Geometry optimizations were done until forces were less than 10^{-5} au and energy convergence by 10^{-8} hartree.

Calculation of the Gibbs free energy (ΔG_B) in the gas phase (without solvent) has been carried out to account for the stability of the metal–TATP complexes. The free energy of binding in gas phase is determined using the electronic energy, zero point energy and entropy terms corresponding to translational, vibrational and rotational motion of the system and enthalpy of reaction. The binding free energy, ΔG_B for Metal–TATP system is calculated for the reaction in Eq. 1 using Eq. 2: where M^{n+} = Cu^{1+}, Li^{1+}, Fe^{2+}, Ni^{2+}, Cr^{2+}, Co^{2+}, Pd^{2+}, In^{3+},Co^{3+},Cr^{3+}, Sb^{3+}, Pd^{4+}, Pt^{4+} and ΔG_B=Free energy of binding in standard state.

$$M^{n+} + TATP \rightarrow [M\text{–}TATP]^{n+} \quad (1)$$

$$\Delta G_B = [M\text{–}TATP]^{n+} - [M^{n+} + TATP] \quad (2)$$

3. Results and discussions

TATP is a 9 member cyclic molecule (Fig. 1a). The calculated lowest energy structures of metal–TATP complexes, as calculated are shown in Fig. 1(b–e). The stable structures (Fig. 1b–e) of metal cations in the center of the TATP ring and binding of metal cation to three alternate oxygen atoms from adjacent peroxide linkage is observed. An isomer of the metal–TATP system where nonalternate-oxygen atoms are bound to the central metal ion was considered in initial study. But energetically the former isomer is more favorable. The later one is less stable by about −10 Kcal/mol considering Zn^{2+} as metal candidate. Hence, it was not considered further. The bonding of oxygen atoms to the metal center is through the donation of lone pair of electrons available on oxygen to the vacant orbitals of the metal ions. This can be rationalized by increase in electronic population in metal valance orbitals and decrease in the same for bound oxygen atoms of TATP. Considering Co^{2+} as an example candidate, the population in Co^{2+} valence orbitals (3d, 4s, 4p) is slightly increased, by about 10% as calculated from natural bond analysis. In certain cases, we observed opening of the TATP ring while complexating with metal cations. For trivalent, tetravalent and divalent (Pd^{2+}, Ni^{2+}) metal–TATP complexes, cleavage of peroxide bonds joining adjacent acetone units is observed (Fig. 1. d and e). The stable products in such cases contain three individual units of acetone peroxide with one oxygen atom bound to the metal center. Alternatively, the cyclic structure of TATP is preserved for monovalent and divalent metal cations complexes with TATP, except for Pd^{2+} and Ni^{2+}.

The calculated geometrical parameters: Bond lengths and bond angles are presented in Table 1. The average value of bond distances for Metal–Oxygen, Metal–Carbon, peroxide bond distance (bound oxygen (O_b, Fig. 1b) to unbound oxygen (O_u, Fig. 1b)) distance, carbon to bound oxygen (O_u), and average angles between O_u–C–O_b and O_u–M–O_b are calculated for different metal-TATP complexes. With complexation, there is an increase in C-O distance and O-O distance by around 10 pms compared to that of bare TATP molecule. However, for metal–TATP complexes with cyclic ring structure of TATP, the C–O_b distance is around 1.5 Å, but for the cleaved complexes the C–O_b distance is around 2.4 Å. The peroxide bond distance O_b–O_u is almost invariant for all the complexes and lies around 1.53 ± 4 Å. The M–O_b bond distance for metal–TATP complexes vary from 1.88 to 2.14 Å (Fig. 2a). This distance correlates with the ionic radii of the corresponding metal ions: increase in ionic radii lead to increase in M–O_u distance. Furthermore, O_b–M–O_u angles change in a more pronounced fashion for different complexes; from the cyclic metal–TATP structure to the metal-fragmented TATP complex the variation is about $\sim 70^\circ$ (Fig. 2b). The similar trend is also observed for O_b–C–O_u angle, but the variation in bond angle is around 40°. The symmetric vibrational stretching frequency (υ) of M–O_b has also been summarized in Table 1. The trend in υ is concomitant with variation in M–O_b bond for the cyclic metal–TATP complexes; longer M–O_u bonds give rise to smaller stretching frequency. However, there are few exceptions noticed for Pd^{2+} and Ni^{2+} TATP complexes.

The electronic charge distribution in the metal–TATP complex (Figs. 3a, b) as obtained from Mulliken and Natural Bond Order (NBO) population analysis shows that the negative charge on the O_b atoms in the metal ion-TATP complex is somewhat larger (30%) than that in the TATP molecule. On the other hand, a decreased charge by 10% on O_u is observed following the ion-TATP complex formation. TATP binding and the amount of charge transfer in the complex exhibits a positive correlation, namely, larger charge transfer corresponding to a stronger binding energy. This correlation suggests that bond formation in the ion-TATP complex includes a large contribution from Coulomb interactions. The binding interaction of metal ion and TATP molecule is presented

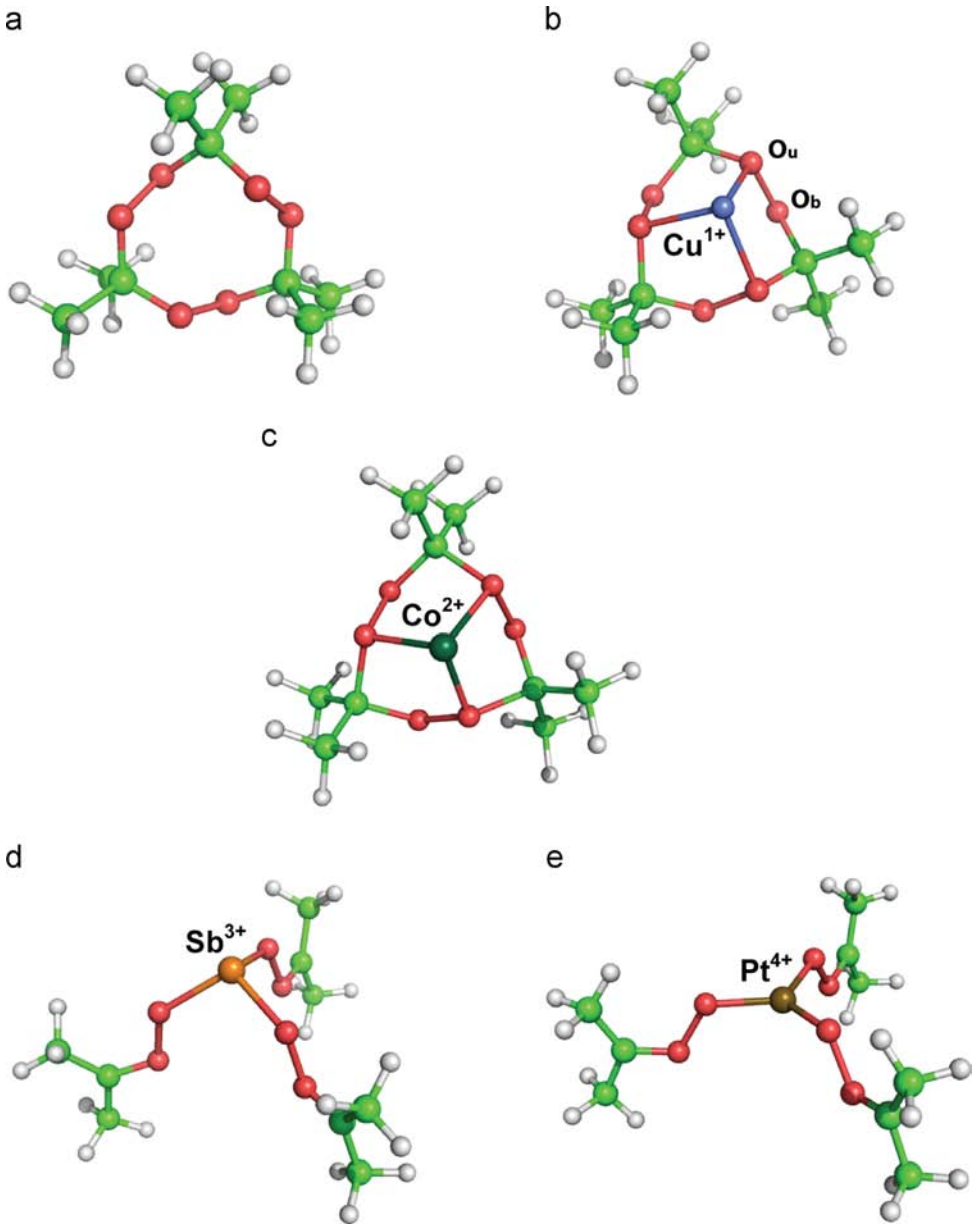

Fig. 1. Image showing DFT (B3LYP/SDD-631 G+(2d) optimized structures of a)TATP and metal-TATP complex b) Cu^{1+}–TATP c) Co^{2+}–TATP d) Sb^{3+}–TATP e) Pt^{4+}–TATP (green = carbon, red = oxygen, white = hydrogen).

Table 1
Ionic radii (IR) of different metal ions, bond distances (Å) and angles (degree), vibrational frequencies of M – Ou bond (ν) in the TATP Molecule, metal ion-TATP complexes, binding free energy (ΔG_B) in Kcal. mol^{-1}, entropy of metal-TATP complexes in Cal. Mol^{-1}. $Kelvin^{-1}$and ΔH in Kcal. mol^{-1} calculated at DFT level of theory with the B3LYP/6-31G**+SDD.

	IR	M–O_b	M–C	O_b–O_u	C–O_b	∟O_b–C–O_u	∟O_b–M–O_u	ν	ΔG_B	S	ΔH
TATP				1.46	1.42	112				125	
CuI	0.77	2.14	2.89	1.54	1.48	109	82	582	93	135	85
LiI	0.76	1.96	2.72	1.54	1.47	109	89	563	102	129	93
ZnII	0.74	2.01	2.79	1.56	1.51	106	90	570	−71	133	-113
CoII	0.72	1.96	2.80	1.55	1.52	104	88	562	−107	135	-80
FeII	0.74	1.89	2.75	1.57	1.53	104	90	564	−104	137	-116
CrII	0.89	1.97	2.80	1.56	1.50	105	86	556	−62	137	-70
NiII	0.69	1.82	3.94	1.52	2.37	36	119	625	−206	150	-142
PdII	0.86	1.97	4.12	1.53	2.42	35	106	595	−171	154	-151
CoIII	0.69	1.73	4.00	1.52	1.33	36	118	678	−664	168	-662
InIII	0.76	2.03	4.15	1.53	1.32	36	120	644	−388	168	-439
CrIII	0.62	1.80	4.05	1.53	2.39	36	119	574	−509	180	-384
SbIII	0.76	2.06	4.46	1.52	2.36	37	106	632	−371	173	-369
PdIV	0.62	1.90	4.20	1.50	2.42	34	120	619	−1317	172	−1314
PtIV	0.63	1.88	4.18	1.57	2.45	36	120	567	−1212	172	−1210

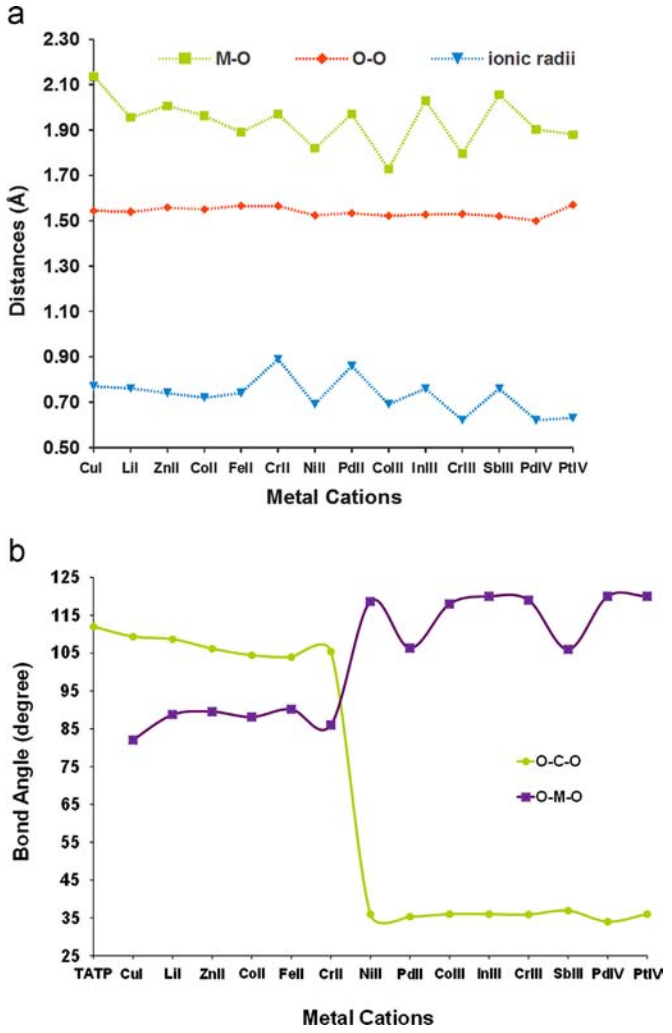

Fig. 2. Plot of variation of (a) ionic radii, bond lengths and (b) bond angles for different metal ions for metal ion-TATPcomplexes vs different metal ions.

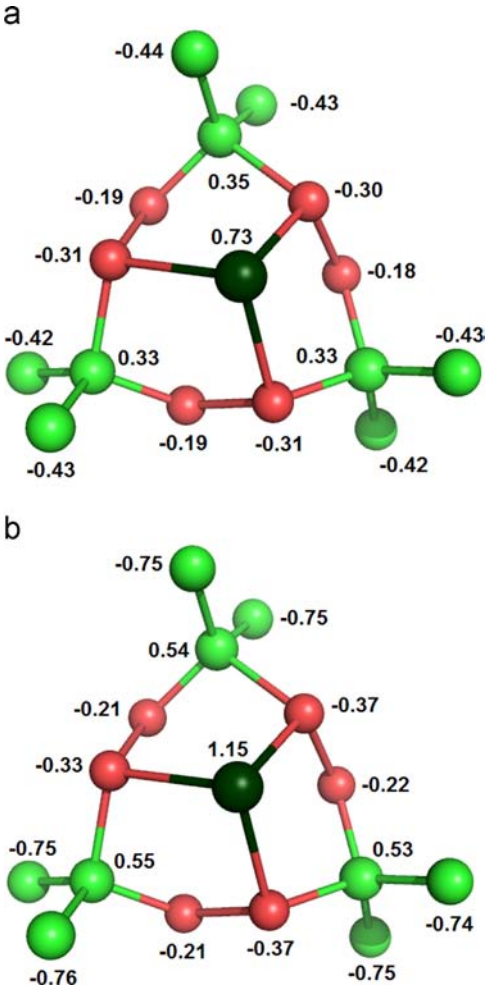

Fig. 3. Charge distribution on different atoms of Co^{2+}–TATP complex calculated from (a) Mulliken and (b) NBO analysis.

through molecular orbital picture (Fig. 4). NBO analysis provides details of electronic distribution in various molecular orbitals of metal–TATP complexes. We notice that the vacant valence orbitals are of s, p, d nature. The population in valence s and p orbitals for different metal complexes is presented in Fig. 5. Comparing the occupancy of molecular orbitals of the metal ion before and after complexation, we see population in valence s and p orbitals for the metal–TATP complexes which were vacant before complexation i. e. in bare metal ion. As a demonstration of this the population in valence shell of Zn^{2+}–TATP complex: 4S(0.13)3d(9.99)4p(0.11); we notice there is population of 1.3% and 1.1% in 4s and 4p orbital respectively compared to zero population in bare Zn^{2+} metal ion, whereas population in 3d orbital shows no variation with complexation. However, in case of Sb^{3+}–TATP complex, the population on Sb^{3+} ion is 5S(1.79)5p(1.01), where there is a large increase in population in p orbital by 11%. This might be the reason for cleavage of TATP cyclic structure.

The free energy of binding computed for different metal-TATP complexes are presented in Table 1. The trend in binding strength shows an increase from monovalent to tetravalent metal ions complexating with TATP: the range in ΔG_B is from 100 Kcal mol^{-1} to -1210 Kcal mol^{-1} (Fig. 6). This wide range can be described by the change in number of electrons in the system, charge as well as the geometry of the complexes. The trend of increase in ΔG_B with increase in ionic radius of the metal ions is noticed (Fig. 7).The ΔG_B is calculated positive for monovalent metal cations such as Li^{1+} and

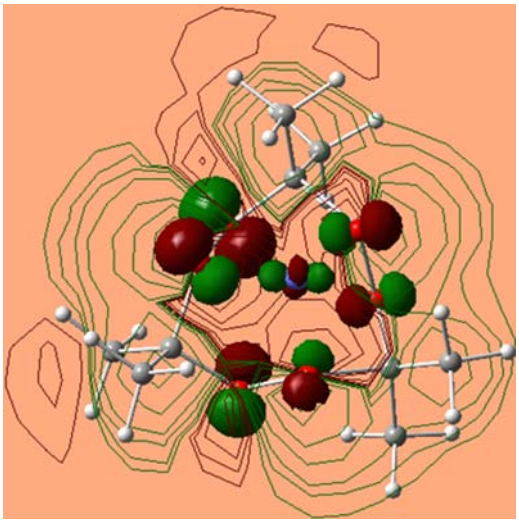

Fig. 4. Molecular orbital of Co^{2+}–TATP (HOMO), showing Co^{2+} binding with TATP molecule.

Cu^{1+}, which shows less probability in complexating TATP. In case of divalent metal ions, the ΔG_B lies around -100 Kcal mol^{-1} or below that except for Pd^{2+} and Ni^{2+} ions, opening of TATP ring structure leads to a different geometry. The trend in stability of the divalent

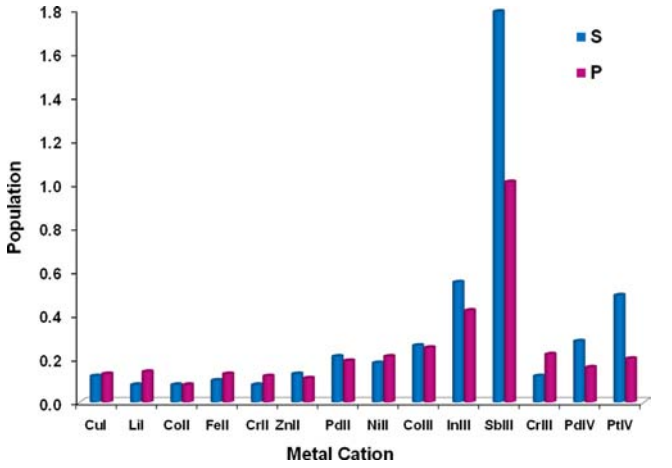

Fig. 5. Population in valence S and P orbital of metal ions calculated from NBO analysis.

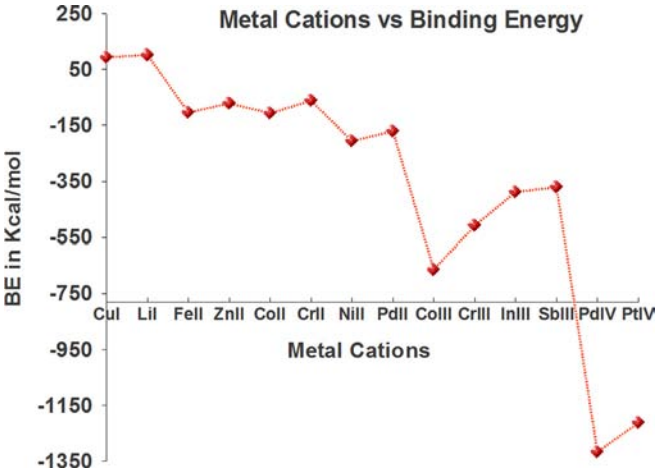

Fig. 6. Graphical presentation of binding free energies (ΔG_B) of Metal ion-TATP complexes vs different metal ions.

metal ions as determined from Table 1 and Fig. 6 is as follows: $Co^{2+} > Fe^{2+} > Zn^{2+} > Cr^{2+}$. According to the results obtained, the strong complexation with $\Delta G_B = -107$ Kcal mol^{-1} is found between Co^{2+} and TATP molecule, followed by Fe^{2+} metal ion with $\Delta G_B = -104$ Kcal mol^{-1}. Even though, the binding energy is high (70–100 Kcal mol^{-1}) in case of Pd^{2+}, Ni^{2+} compared to other divalent metal ions, they need to be considered carefully for their complexation result bonding with the fragments of TATP. The free energy of complexation for trivalent metal ions is spread over a range from -371 to -664 Kcal mol^{-1}. The trivalent metal–TATP complexes are calculated with cleaved TATP ring structure (Fig. 1d). Hence, in this case the ionic radii of the metal ions are crucial in determining the free energy variation. The trend in stability of these metal–TATP complexes is $Co^{3+} > Cr^{3+} > In^{3+} > Sb^{3+}$. Similar to the trivalent metal ions tetravalent ions also exhibit cleaved TATP ring (Fig. 1e). The ΔG_B is the highest in the series of metal ions studied: Pd^{4+}–TATP is the complex with highest $\Delta G_B = -1314$ Kcal mol^{-1} followed by Pt^{4+} with -1210 Kcal mol^{-1}.

The enthalpy of reaction (ΔH) and total entropy (ΔS) of the metal–TATP complexes are also presented in Table 1. The enthalpy of formation (ΔH) of metal TATP-complexes are negative; this confirms the feasibility of complexation of TATP to different metal ions. The trend of ΔH is concomitant with the free energy change ΔG_B. The increase in entropy for the complexes with decrease in metal ionic radii from monovalent metal-TATP complex to tetravalent metal-TATP complex there is an increase in entropy by 40 cal mol^{-1} K^{-1}. In addition the cleavage of TATP ring leads to increase in entropy for the metal–TATP complexes. For divalent metal–TATP complexes, where the TATP ring is raptured, there is an increase in entropy by 20 cal mol^{-1} K^{-1}.

However, for determination of stability of the complex of TATP with metal ions we excluded the complexes with cleaved TATP ring structure, because during complexation the target molecule undergoes change and do not retain the stating structure. Hence,

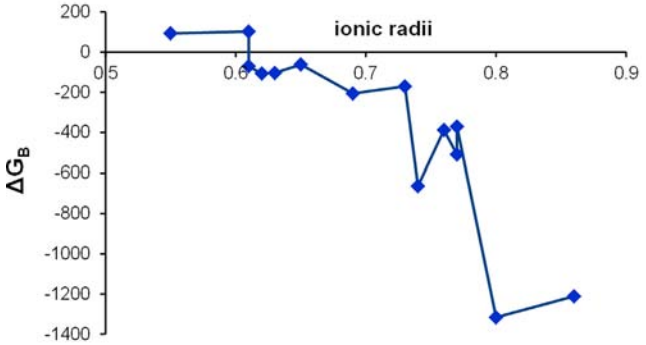

Fig. 7. Variation in free energy of binding (ΔG_B) of metal–TATP complexes with respect to the ionic radius of metal ions.

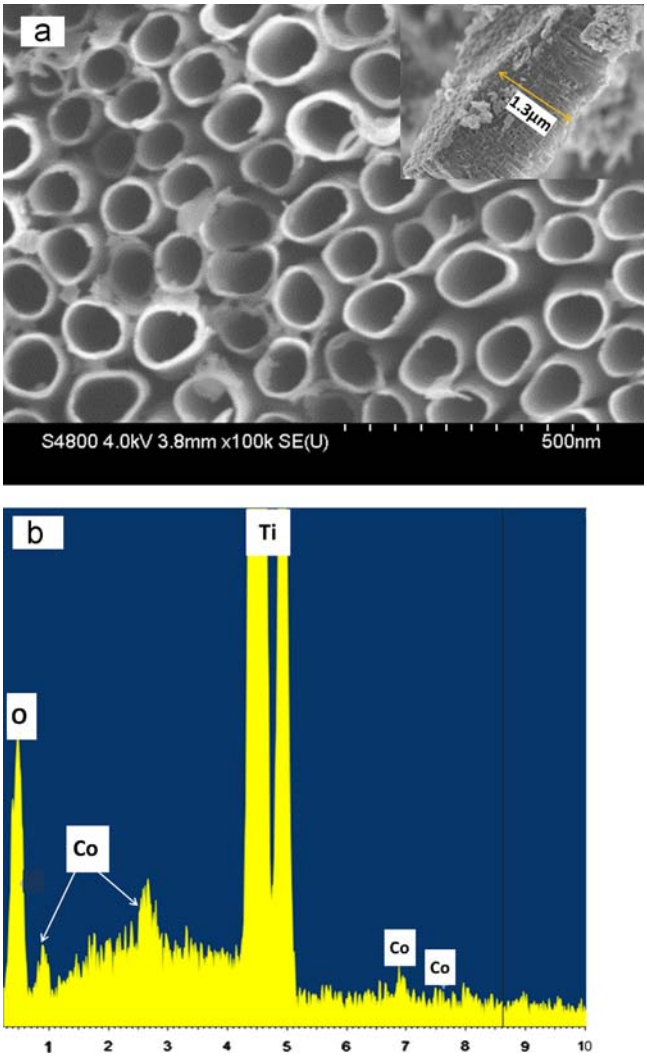

Fig. 8. (a) SEM image of Co^{2+} functionalized T–NT and (b) EDS image showing the composition of the material.

the monovalent and divalent metal cations except Pd^{2+} and Ni^{2+} such as Co^{2+}, Fe^{2+}, Zn^{2+}, Cr^{2+}, Cu^{1+}, Li^{1+} are only considered and the trend ($Co^{2+} > Fe^{2+} > Zn^{2+} > Cr^{2+} > Cu^{1+} > Li^{1+}$) in ΔG_B for these complexes decide the stability of the complexes. The present study show Co^{2+} will be the suitable metal ion with a high propensity for complexing with TATP.

4. Experimental studies

Various research groups have been involved in the development of new synthesis and fabrication methods to prepare TiO_2–NT-arrays (both hexagonal and circular) with controlled morphology and material properties [24-27]. In this study, TiO_2–NT arrays were prepared by potentiostatic anodization in an electrolyte consisting of ethylene glycol (EG), 0.5 wt% ammonium fluoride, and 10% H_2O. Prior to anodization, the electrolyte was aged for at least 48 h in a sealed container. Anodization was carried out with a DC power source (Agilent Technologies E3647A) connected to a titanium coupon (anode) and a platinum (cathode). The electrolyte was stirred at 90-rpm. The anodization was carried out at a constant voltage of 40 V for 30 min at room temperature. After the anodization, the coupon was removed and cleaned by sonication for 3–5 s in de-ionized water and dried at 100 °C for 1 h in air. Annealing was performed in a tube furnace in oxygen environment at 500 °C. The annealing process converts the

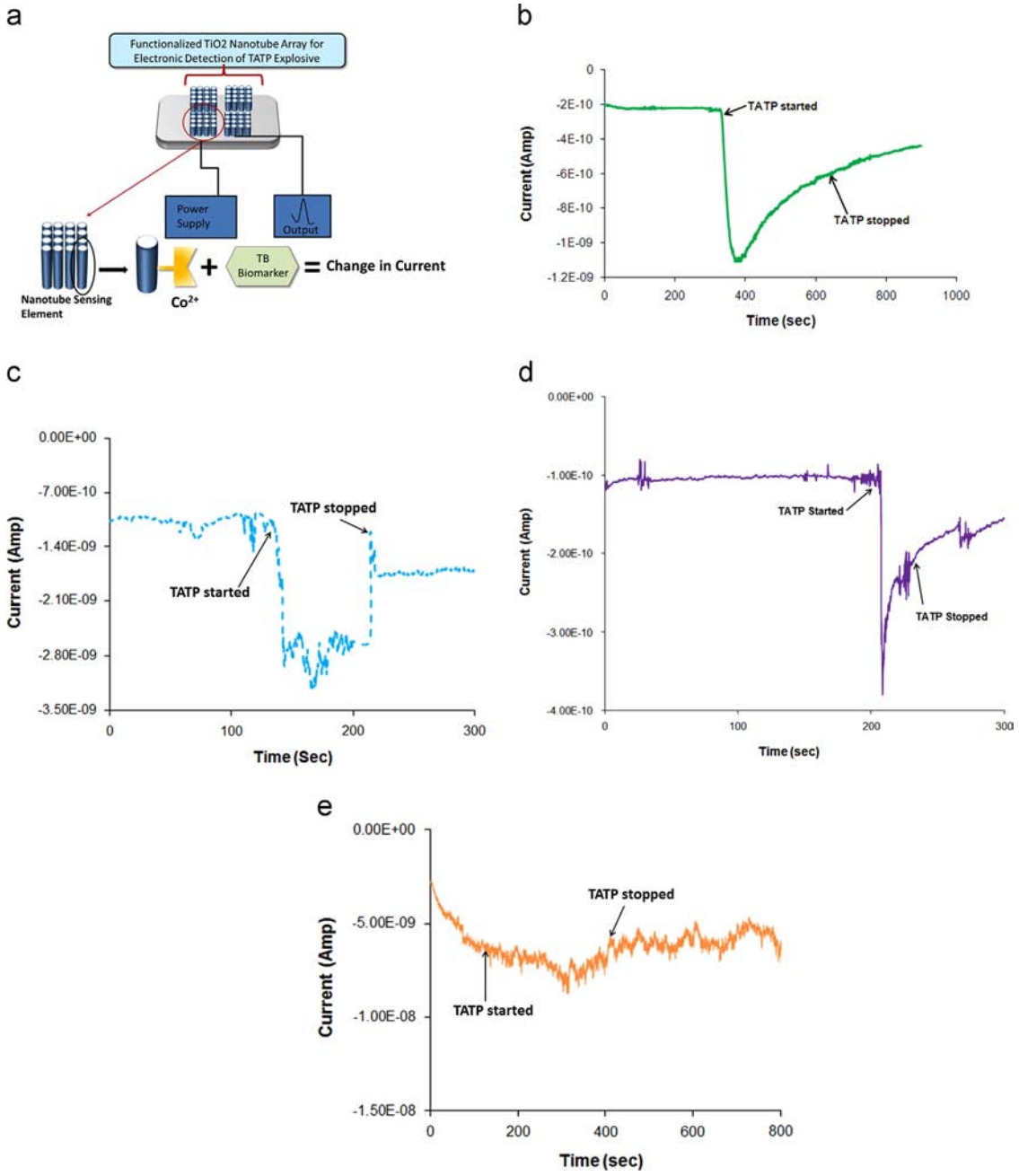

Fig. 9. (a) Schematic showing Co^{2+} functionalized TiO_2 sensor for TATP detection. (b) Potentiostatic (I–t) plot of Co–TiO_2 detector with and without TATP vapor. The plot shows there is a change in current obtained after passing TATP vapors, current obtained after the removal of the TATP source from Co–TiO_2 sample. An increase in negative current shows the complexation of TATP on the TiO_2 nanotube sensor. Preliminary investigations showing similar plots (I–t) for (c) Fe–TiO_2 sample, (d) Cr–TiO_2 sample, and (e) Cu–TiO_2 sample upon passing TATP vapor. Comparison of these plots demonstrates varied current responses of the sensor platform based on different metals ions present on the platform.

amorphous, as formed TiO_2–NT phase to a crystalline phase [25]. The temperature was raised at a rate of 1.5 °C/min to the set point and maintained for 2 h. After holding the anodized sample at the elevated temperature, the samples were allowed to cool within the furnace by natural convection. During this whole process, oxygen gas was continuously supplied through the furnace tube to maintain the oxygen rich atmosphere to make the TiO_2–NT phase relatively more resistive [14].

Chemical Deposition of Co^{2+}: Based on the results obtained from computational studies, presented above, Co^{2+} has been selected as the candidate metal. Experiments are performed to functionalize TiO_2–NT surface with Co^{2+} metal ions. Co^{2+} functionalization of TiO_2–NT was done by sonication of the anodized samples immersed in a dilute cobalt nitrate solution.

4.1. Characterization

Examination of the morphology (surface and cross section) for the TiO_2–NT was performed using a field emission scanning electron microscope (Hitachi S-4800). EDS analysis was done using oxford system (X-Max) attached to the Hitachi S-4800 SEM system. Fig. 8 (a) shows the self-organized and vertically aligned architecture of the TiO_2–NT array structure formed on the titanium foil by anodization at 40 V for 30 min. The nanotubes were found to have an average diameter of ~80 nm, length of ~1.3 μm (inset Fig. 8(a)) and wall thicknesses in the range of 15–20 nm. The EDS spectrum, shown in Fig. 8(b) demonstrates the presence of Co on the TiO_2–NT surface.

5. TATP detection study

Fig. 9a shows the test setup for detecting TATP using functionalized TiO_2 nanotube arrays. The sensor array was constructed on a planar titanium substrate. Two copper electrical leads were connected to the each side of the sensor using a standard silver epoxy. The leads were connected to a potentiostat that provides a bias voltage to the sensor and measures the current. The sensing studies of the Co^{2+}–TiO_2 material were carried out under nitgen atmosphere. The bias voltage for sensing measurement was determined to be −0.5 V from the current–voltage curve for Co^{2+}–TiO_2 system. Current measurements were taken with and without passing TATP vapors through the sensor material at –0.5 V. The current measured at –0.5 V bias without exposure to TATP was considered as the background current. The sensor was exposed to TATP vapor by placing 5 mg of TATP in a 50 ml flask and passing the vapor generated from the TATP through a 1 mm diameter glass nozzle. The change in background current is indicative of complexation of TATP with metal cations adsorbed on the nanotubes. Compared to the base line current measured without passing TATP vapors (resistivity of the metal–TiO_2–NT), there was a sharp change in the current (by a factor of 6) when the sensor material was exposed to TATP vapor (shown in Fig. 9b). The current signal remained around that level until the TATP exposure was continued. It goes back towards the base line once TATP source is removed. A similar change in signal was observed when the nanotubes functionalized with Co^{2+} were exposed to TATP vapors under ambient conditions. For comparative purposes, we have also conducted similar investigations of the interaction of TATP with Fe^{2+}–TiO_2–NT, Cr^{2+}–TiO_2–NT, and Cu^{+}–TiO_2–NT arrays. The representative current response profiles for these experiments are shown in Fig. 9(c–e). It can be observed that that changes in current response varies depending on the type of metal ion present in the TiO_2–NT substrate. The results are consistent with the theoretical analysis as described above. A detailed experimental investigation of the interactions of various metal ions-sensitized TiO_2–NT with TATP vapor will be a promising avenue for future study and will be communicated later.

The results show that it is feasible to develop a solid state sensor for detection of TATP based on metal functionalized TiO_2–NT. The sensor gave a positive response through change in conductivity, once the metal coating on to the TiO_2 nanotubes bound to the peroxide molecules. This increase in conductivity was measured by applying an external bias (0.5 V) and taking simple current readings. The increase in current was proportional to the concentration of the explosive molecule adsorbed on the surface of the nanotube.

From the combined theoretical and consequent experimental studies, it is clear that metal sensitized TiO_2 nanostructure can serve as a sensor platform in detecting peroxide based explosive TATP. However, our preliminary computational results are limited to selection of metal ion Co^{2+} without any TiO_2 surface attached to it. The interaction of TATP with metal ions attached to extended periodic TiO_2 surface would be the more comparable model to the sensor platform designed to detect the explosive material. Hence, detailed theoretical study considering stable TiO_2 anatase (101) surface [28,29] with variable slab size needs to be considered, brief comparison to previous calculations without TiO_2 surface will provide the effect of solid substrate. In addition, the experimental study performed for this communication need to be done more rigorously using different concentration of TATP, which can provide details about the sensitivity of the sensor device. These concentrations will be from 100 ppm down to 1 ppb. The goal is to optimize the sensor for detection of levels at the 1 pbb or lower which should be sufficient to detect low levels of TATP and other types of explosives. To characterize the sensor performance in various environmental conditions as the target use of the sensor is all over the world where humidity and temperature can vary. In addition selectivity and sensitivity of the sensor will be characterized in presence of ambient air which contains many volatile organic compounds. The parameters must be characterized and optimized so the sensor will handle a real world sample.

Acknowledgment

An allocation of computer time from the Center for High Performance Computing at the University of Utah is gratefully acknowledged. We greatly acknowledge Prof. Keith Prisbrey for his suggestions and support.

References

[1] L. Pacheco-Londoño, O. M. Rimera, M. Ramírez, O. Ruiz, S. Hernandez-Rivera, in: E.M. Carapezza, Proceedings of the International Society for Optics and Photonics SPIE '05, vol no. 5778, 2005 pp. 317–326.
[2] Z. Takats, I. Cotte-Rodriguez, N. Talaty, H. Chen, R.G. Cooks, Chem. Commun. (2005) 1950–1952.
[3] E. Keinan, H. Itzhaky, Chem. Abstr. 131 (1999) 172322–172329.
[4] W.H. Zhang, W.D. Zhang, L.Y. Chen, Nanotechnology 21 (2010) 315502–315507.
[5] R.I. Hiyoshi, akamura, Propellants Explos. Pyrotech. 32 (2007) 127–134.
[6] J.S. Yang, T.M. Swager, J. Am. Chem. Soc. 120 (1998) 5321–5322.
[7] I. Cotte-Rodríguez, H. Hernandez-Soto, H. Chen, R.G. Cooks, Anal. Chem. 80 (2008) 1512–1519.
[8] R. Schutte-Ladbeck, M. Vogel, U. Karst, Anal. Bioanal. Chem. 386 (2006) 559–565.
[9] F. Dubnikova, R. Kosloff, Y. Zeiri, Z. Karpas, J. Phys. Chem. A 106 (2002) 4951–4956.
[10] G. Harsanyi., Sen. Rev. 20 (2000) 98–105.
[11] G.K. Mor, O.K. Varghese, M. Paulose, K. Shankar, C.A. Grimes, Sol. Energy Mater. Sol. Cells 90 (2006) 2011–2075.
[12] N.R. De Tacconi, C.R. Chenthamarakshan, G. Yogeeswaran, A. Watcharenwong, R.A. De Zoysa, N.A. Basit, K. Rajeswar, J. Phys. Chem. B 110 (2006) 25347–25355.
[13] S.K. Mohapatra, V.K. Mahajan, M. Misra, Nanotechnology 18 (2007) 445705–445710.
[14] S. Banerjee, S. Mahapatra, M. Misra, I.B. Ghosh, Nanotechnology 20 (2009) 075502–075508.

[15] B. Sarma, A.L. Jurovirtski, R.S. Ray, Y. Smith, S. Mohanty, M. Misra, J. Power Sources, 236(2013) 113.
[16] B. Sarma, Y. Smith, S. Mohanty, M. Misra, Mater. Lett. 85 (2012) 33.
[17] Y. Smith, R.S. Ray, K. Carlson, B. Sarma, M. Misra, Materials 6 (2013) 2892.
[18] Y. Smith, B. Sarma, S. Mohanty, M. Misra, ACS, Appl. Mater. Interaces 4 (2012) 5883.
[19] B. Sarma, Y. Smith, A.L. Jurovirtski, S. Mohanty, M. Misra, ACS, Appl. Mater. Interfacesd 5 (2013) 1688.
[20] Y. Smith, B. Sarma, S. Mohanty, M. Misra, Electrochem. Commun. 19 (2012) 131.
[21] Y. Smith, B. Sarma, S. Mohanty, M. Misra, J. Int, Hydrogen Energy 38 (2013) 2062.
[22] M.J. Frisch, G.W. Trucks, H.B. Schlegel, G.E. Scuseria, M.A. Robb, J.R. Cheeseman, G. Scalmani, V. Barone, B. Mennucci, G.A. Petersson, H. Nakatsuji, M. Caricato, X. Li, H.P. Hratchian, A. F. Izmaylov, J. Bloino, G. Zheng, J.L. Sonnenberg, M. Hada, M. Ehara, K. Toyota, R. Fukuda, J. Hasegawa, M. Ishida, T. Nakajima, Y. Honda, O. Kitao, H. Nakai, T. Vreven, J. A. MontgomeryJr., J.E. Peralta, F. Ogliaro, M. Bearpark, J. J. Heyd, E. Brothers, K.N. Kudin, V.N. Staroverov, R. Kobayashi, J. Normand, K. Raghavachari, A. Rendell, J. C. Burant, S.S. Iyengar, J. Tomasi, M. Cossi, N. Rega, J.M. Millam, M. Klene, J. E. Knox, J.B. Cross, V. Bakken, C. Adamo, J. Jaramillo, R. Gomperts, R.E. Stratmann, O. Yazyev, A.J. Austin, R. Cammi, C. Pomelli, J.W. Ochterski, R.L. Martin, K. Morokuma, V.G. Zakrzewski, G.A. Voth, P. Salvador, J.J. Dannenberg, S. Dapprich, A.D. Daniels, Ö. Farkas, J. B. Foresman, J.V. Ortiz, J. Cioslowski, D.J. Fox, Gaussian 09, Revision A.1, Gaussian, Inc., Wallingford CT, 2009.
[23] X. Xu, D.G. Truhlar, J. Chem. Theory Comput. 8 (2012) 80–90.
[24] S.K. Mohapatra, M. Misra, V.K. Mahajan, K.S. Raj, J. Catal. 246 (2007) 362–369.
[25] K.S. Raja, M. Misra, K. Paramguru, Electrochim. Acta 51 (2005) 154–165.
[26] S.K. Mohapatra, M. Misra, J. Phys. Chem. C 111 (2007) 11506–11510.
[27] K.S. Raja, T. Gandhi, M. Misra, Electrochem. Commun. 9 (2007) 1069–1076.
[28] F. Labat, P. Baranek, C.J. Adamo, Chem. Theory Comput. 4 (2008) 341–352.
[29] V.M. Bermudez, J. Phys. Chem. C. 114 (2010) 3063–3074.